Annealing properties of vacancy-type defects in ion implanted GaN during ultra-high-pressure annealing studied by using a monoenergetic positron beam

Akira Uedono*[1], Hideki Sakurai[2,3,†], Jun Uzuhashi[4], Tetsuo Narita[5], Kacper Sierakowski[6], Shoji Ishibashi[7], Shigefusa F. Chichibu[8], Michal Bockowski[2,6], Jun Suda[2], Tadakatsu Ohkubo[4], Nobuyuki Ikarashi[2], Kazuhiro Hono[4], and Tetsu Kachi[2]

[1]Faculty of Pure and Appl. Sci., Uni. of Tsukuba, Tsukuba, Ibaraki 305-8573, Japan; [2]Nagoya Univ., Aichi 464-8601, Japan; [3]AIT, ULVAC, Inc., Chigasaki, Kanagawa 253-8543, Japan; [4]National Inst. for Materials Sci., Tsukuba 305-0047, Japan; [5]Toyota Central R&D Labs., Inc., Nagakute, Aichi 480-1192, Japan; [6]Inst. of High Pressure Phys., Polish Academy of Sciences, Sokolowska 29/37, 01-142 Warsaw, Poland; [7]Research Center for Computational Design of Advanced Functional Materials, AIST, Tsukuba, Ibaraki 305-8568, Japan; [8]Inst. of Multidisciplinary Research for Advanced Materials, Tohoku Univ., Sendai 980-8577, Japan

ABSTRACT

Behaviors of vacancy-type defects in ion-implanted GaN were studied by means of positron annihilation. Si or Mg ions were implanted into GaN to obtain 300-nm-deep box profiles of the impurities. The ion-implanted samples were annealed up to 1480°C under a N_2 pressure of 1 GPa (ultra-high-pressure annealing: UHPA). For as-implanted GaN, the major defect species was identified as Ga-vacancy-type defects such as a divacancy ($V_{Ga}V_N$). After annealing above 1000°C, vacancy clusters, such as $(V_{Ga}V_N)_3$, were introduced, and they were found to be remained even after 1480°C annealing. For Mg-implanted GaN with [Mg]=10^{18} cm^{-3}, no large change in the depth distribution of Mg was observed before and after annealing at 1400°C. For the sample with [Mg]=10^{19} cm^{-3}, however, Mg diffused into the bulk, which was attributed to the over-doping of Mg and their vacancy-assisted diffusion. The Mg diffusion was suppressed by sequential N-implantation, which was attributed to the reaction between Mg and vacancies under a N-rich condition. Interactions between vacancies, Mg, and H during UHPA were also discussed.

Keywords: GaN, ion implantation, defect, vacancy

1. INTRODUCTION

GaN based devices have attracted attention because of its excellent electrical properties.[1,2] Recently, vertical GaN power devices have studied significantly because of their high break down voltage and their reliability.[3,4] It was suggested that ion implantation is an indispensable technique to fabricate p-type regions in these vertical power devices.[5,6] However, a drawback of the impurity doping using ion implantation is the introduction of point defects. Thus, R&D of annealing processes is a key to develop the GaN-based vertical devices.[7-12] Sakurai *et al.*[10] reported that a high activation rate for Mg can be obtained by using an ultra-high-pressure annealing (UHPA), where annealing was done with an N_2 pressure of 1 GPa at up to 1480°C. Since many kinds of defects are introduced by ion implantation and post-implantation annealing,[6] a study of annealing behaviors of defects, such as agglomeration of vacancies and their dissociation, is important for utilizing ion implantation for GaN devices. Positron annihilation is a useful technique for a study of vacancy-type defects in semiconductors. [13,14] This technique has been successfully used to detect vacancy-type defects in GaN.[15-18] In the present study, we used a monoenergetic positron beam to study the annealing behaviors of vacancy-type defects in ion-implanted GaN with UHPA.[19,20]

*uedono.akira.gb@u.tsukuba.ac.jp

[†]Present address: Electronic Devices & Storage Research & Development Center, Toshiba Electronic Devices & Storage Co.

2. EXPERIMENT

The samples used in the present experiments were undoped 1.7-μm-thick GaN films grown by MOVPE. Mg^+ ions were implanted into the samples to obtain 300-nm-deep box profiles with [Mg]= 1×10^{18} cm^{-3} and 1×10^{19} cm^{-3}, respectively. The samples were annealed at temperatures between 1000°C and 1480°C (5 min) under a N_2 pressure of 1 GPa using a high-nitrogen-pressure solution system.[21] For the sample with [Mg]=1×10^{19} cm^{-3}, N^+ ions were sequentially implanted after Mg-implantation in order to obtain a 300-nm-deep box profile with [N]=1×10^{19} cm^{-3}. Si^+ ions were also implanted into GaN to obtain 300-nm-deep box profiles with [Si]=1×10^{19} cm^{-3}.

Details on the positron annihilation technique are described elsewhere.[13,14] When a positron is implanted into solids, it annihilates with an electron and emits γ quanta (Fig. 1). The energy distribution of the γ rays is broadened by the momentum component of the annihilating electron-positron pair p_L. A freely diffusing positron could be trapped by a vacancy because of Coulomb repulsion from ion cores. Because the momentum distribution of the electrons in defects differs from that of electrons in the bulk, the defects can be detected by measuring Doppler broadening spectra of the annihilation radiation. The change in the spectra due to the positron trapping is shown in Fig. 2. In the present experiments, the Doppler broadening spectra of the annihilation radiation were measured with Ge detectors as a function of the incident positron energy *E*. They were also measured with a coincidence system.[13,14] The obtained *S*–*E* curves

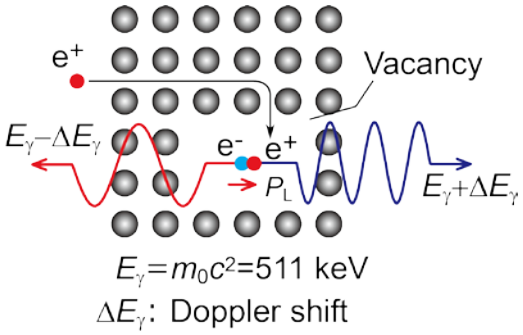

Fig. 1. Positron annihilates with electron producing γ rays (511 keV). When positrons are implanted into solids, they could be trapped by vacancy-type defects. From energy distribution of annihilation γ rays due to the annihilation of positrons with electrons in the defect, one can detect vacancy-type defects.

Fig. 2. Schematic drawing of Doppler broadening spectrum for (a) annihilation of positrons in free state and for annihilation of positrons trapped by (b) monovacancy and (c) vacancy cluster. Doppler broadening spectrum is characterized by *S* and *W* parameters.

were analyzed by VEPFIT, a computer program developed by van Veen *et al*.[22] Doppler broadening spectra corresponding to a delocalized positron and to positrons trapped by typical cation vacancies were calculated using the QMAS (Quantum MAterials Simulator) code.[23] Details of the simulation are given elsewhere.[23,24]

3. RESULTS AND DISCUSSION

Figure 3 shows the *S* values of Si-implanted GaN before and after UHPA at 1000–1480°C as a function of *E*. The mean positron implantation depth is shown on the upper horizontal axis. For the as-implanted sample, the *S* value increases as *E* decreases at *E*=0.1–3 keV, which is due to the annihilation of positrons at the surface. In the region between *E*=3–10 keV, the *S* value is almost constant, and it is higher than the *S* value for the high-quality GaN that shows no defect response (0.442), suggesting the annihilation of positrons trapped by vacancy-type defects introduced by Si-implantation. After annealing at 1000°C, the *S* value at *E*≅6 keV increased. This is due to the agglomeration of vacancies and the annihilation of positrons by large vacancy clusters. After annealing at 1400–1480°C, the *S* value started to decrease, but it was still higher than that for the as-implanted sample.

Fig. 3. *S*–*E* relationships for Si-implanted GaN before and after UHPA. Annealing temperatures are shown in figure. Solid curves are fits to experimental data, and derived depth distributions of *S* are shown in Fig. 4. Arrow shows *S* for defect-free GaN.

Solid curves in Fig. 3 are fits to the experimental data, and the derived depth distributions of *S* and Si determined by SIMS are shown in Fig. 4. It can be seen that the depth distribution of Si for the annealed sample is almost identical to that for the sample before annealing. The distribution of vacancies shifts toward the surface by annealing, as a result, an agglomeration occurred in the subsurface region (≤ 400°C).

The defect species can be identified from the relationship between *S* and *W* paramters.[13,14] Figure 5 shows the relationship between *S* and *W* for Si-implanted GaN before and after UHPA. The spectra were measured at *E*=6 keV. The (*S*,*W*) value corresponding to the positron annihilation in defect-free (DF) GaN is shown as "DF" in the figure. The calculated (*S*,*W*) value for the annihilation of positrons in the delocalized state is shown as "DF(cal.)". The (*S*,*W*) values obtained from the simulation for the annihilation of positrons trapped by vacancy-type defects, such as Ga-vacancy V_{Ga}, and their complexes with V_N [$V_{Ga}(V_N)_n$ (n=1–3), $(V_{Ga}V_N)_2$, and $(V_{Ga}V_N)_3$] are also shown (blue symbols). For the as-implanted sample, the (*S*,*W*) value is close to the calculated values for V_{Ga} and $V_{Ga}V_N$. Thus, the major defect species in the as-implanted sample can be identified as V_{Ga}-related defects. After annealing at 1000–1100°C, the (*S*,*W*) value shifts to the right-hand side and locates on the line connecting the (*S*,*W*) value for defect-free GaN and $(V_{Ga}V_N)_3$. Above 1200°C annealing, the observed (*S*,*W*) values locate on the right-hand side of the line, suggesting a further increase in the size of vacancy-type defects. These results suggest that vacancy clusters, such as$(V_{Ga}V_N)_3$, are formed during annealing process and they remained even after UHPA at 1480°C.

Figure 6 shows the *S*–*E* relationships for Mg-implanted GaN with [Mg] = 10^{18} cm^{-3} before and after UHPA. For the as-implanted sample, the *S* value at *E*≅6 keV is close to that for the Si-implanted GaN before UHPA, suggesting that the major defect species is V_{Ga}-related defects. After annealing at 1200°C, the *S* value corresponding to the positron

Fig. 4. Depth distributions of *S*, Si and H for Si-implanted GaN before and after UHPA at 1400°C.

Fig. 5. *S*–*W* relationships for Si-implanted GaN (brown symbols). Annealing temperatures are shown in figure. (*S*,*W*) for unimplanted GaN is shown as "DF" (defect-free). (*S*,*W*) obtained by simulations for defect-free GaN [DF(cal.)], V_{Ga}, $V_{Ga}(V_N)_n$ (n = 1–4), $(V_{Ga}V_N)_2$, and $(V_{Ga}V_N)_3$ are shown as blue symbols

annihilation in the subsurface region (E=2–9 keV) started to decrease. A similar annealing behavior for *S* has been reported in the previous works.[19,25-27] After annealing at a high temperature, Mg atoms are partially activated and cause a downward shift in the Fermi level position. Thus, the charge states of vacancy-type defects tend to be positive after annealing. The trapping rate of positrons for positively charged vacancies is low because of Coulomb repulsion between them.[13] The observed decrease in the *S* value, therefore, is not due to the annealing out of vacancies but the shift in the defect charge state from neutral (negative) to positive (neutral) (ex. $V^0 \rightarrow V^+$).

The depth distributions of *S* for the samples with [Mg]=10^{18} cm^{-3} before and after UHPA are shown in Fig. 7(a). These from the *S*–*E* relationships for Mg-implanted GaN with [Mg]=10^{19} cm^{-3} and Mg-implanted GaN with sequential N-implantation are shown in Fig. 7(b) and (c), respectively. Depth distributions of Mg for these samples are shown in Fig. 7(d), (e), and (f). For Mg-implanted GaN with sequential N-implantation, the depth profile of implanted N calculated by using SRIM code[28] is shown in Fig. 7(f). The incorporation of H into Mg-implanted GaN was reported to start after UHPA above 1000°C.[19] The depth profiles of H after UHPA at 1400°C are also shown in Fig. 7(d), (e), and (f). For the samples with [Mg]=10^{18} cm^{-3}, no large change is observed in the depth distributions of Mg before and after UHPA at 1400°C. For the samples with [Mg]=10^{19} cm^{-3}, however, Mg diffused into the bulk, and its distribution extended around 1 μm after annealing. For this sample, [Mg] in the box profile was close to the doping threshold of Mg (1–3×10^{19} cm^{-3}),[29] and this concentration is likely to be the solubility limit of Mg in GaN. Thus, excess Mg atoms in the box profile could diffuse into deeper region during the annealing. As shown in Fig. 7(b) and (c), the depth profile of vacancy-type

Fig. 6. *S*–*E* relationships for Mg-implanted GaN with [Mg]=10^{18} cm^{-3}. Derived depth distributions of *S* are shown in Fig. 7(a).

Fig. 7. Depth distributions of *S* for Mg-implanted GaN with [Mg]= (a) 10^{18} cm^{-3} and (b) 10^{19} cm^{-3}, and (c) those of *S* for Mg-implanted GaN after N-implantation ([Mg]=10^{19} cm^{-3}). Depth distributions of Mg, H, and N are shown in (d), (e), and (f).

defects in the as-implanted sample reaches around 1300 nm. Based on the results obtained for Si-implanted GaN, such defects are unlikely to be fully annealed out at this temperature range. Thus, although the *S* value around 1 μm is close to the defect-free *S* value [Fig. 7(b)], a certain number of vacancies could exist in this region. The distortion of the Mg profile after UHPA at 1400°C, therefore, is considered to be driven by vacancy-assisted diffusion.

As shown in Fig. 7(e), the depth distribution of H is close to the Mg depth profile for the sample annealed at 1400°C, and its concentration almost coincides with [Mg] below 400 nm. Using hybrid functional calculations, Lyons *et al*.[30] reported that the formation energy of Mg at a Ga site is decreased by pairing with H if the Fermi level locates below the middle of the bandgap. From a combination of first-principles calculations, Lee *et al*.[31] suggested that Mg-H-V_N complexes are one of the common forms of Mg in GaN. Because the vacancy-rich region extends up to 1 μm [Fig. 7(b)], the Mg and H atoms that diffuse into this region can couple with vacancies, and this is considered to be the origin of the coincidence of the depth profile for Mg and H for the sample annealed at 1400°C.

For the sample with sequential N-implantation [Fig. 7(f)], although the relationship between H and Mg is similar to that for the sample without the N-implantation, [Mg] is higher than [H] in the region corresponding to the box profile of N (≤400 nm). This suggests that the formation of Mg and H complexes is suppressed in this region. From annealing experiments for N-implanted GaN,[32] it was found that N-implantation decreased the size of vacancy clusters above 1200°C annealing. This fact was attributed to the decrease in the number of V_N due to the recombination between V_N and excess N atoms. As shown in Figs. 7(b) and (c), for the sample with the sequential N-implantation after annealing at 1200°C, the *S* value in the subsurface region (≤ 400 nm) is smaller than that for the sample without the N-implantation, suggesting the suppression of vacancy cluster formation. This defect reaction could decrease the possibility of H by being trapped vacant N sites near Mg. Thus, in the region with high [N], the formation of Mg-H-V_N is considered to be suppressed, and the imbalance between cation and anion vacancies could increase the number of Mg without forming Mg-H pairs.

The present work showed that the vacancy-type defects introduced by ion implantation exist even after UHPA at 1480°C, and they are expected to play a critical role in the formation of secondary defects and their atomic configuration.[20,33] Thus, knowledge on defect reactions revealed by the combination of characterization techniques used in the present work will shed light on finding appropriate annealing parameters for the fabrication of p-type GaN by Mg-implantation.

Acknowledgement

This work was supported in part by the NEDO Program for Cross-ministerial Strategic Innovation Promotion, the MEXT Program for Research and Development of Next-Generation Semiconductor to Realize Energy-Saving Society (JPJ005357), the MEXT Program for Creation of Innovative Core Technology for Power Electronics (JPJ009777), and JSPS KAKENHI (JP16H06424 and 21H01826). This research was also partially supported by Polish National Centre for Research and Development through project TECHMATSTRATEG-III/0003/2019-00 and Polish National Science Centre (NCN) through project 2018/29/B/ST5/00338.

REFERENCES

[1] B. J. Baliga, Semicond. Sci. Technol. **28**, 074011 (2013).
[2] A. Lidow, J. Strydom, M. De Rooij, D. Reusch, GaN Transistors for Efficient Power Conversion, John Wiley & Sons (2014).
[3] H. Amano *et al*., J. Phys. D: Appl. Phys. **51**, 163001 (2018).
[4] J. Hu, Y. Zhang, M. Sun, D. Piedra, N. Chowdhury, T. Palacios, Mat. Sci. Semi. Process. **78**, 75-84 (2018).
[5] S. J. Pearton, J. C. Zolper, R. J. Shul, and F. Ren, J. Appl. Phys. **86**, 1 (1999).
[6] S. O. Kucheyev, J. S. Williams, and S. J. Pearton, Mat. Sci. Eng. **33**, 51-107 (2001).
[7] J. D. Greenlee, T. J. Anderson, B. N. Feigelson, K. D. Hobart, and F. J. Kub, Phys. Stat. Sol. A 212, 2772-2775 (2015).
[8] T. Oikawa, Y. Saijo, S. Kato, T. Mishima, and T. Nakamura, Nucl. Inst. Meth. B **365,** 168-170 (2015).
[9] T. Narita, T. Kachi, K. Kataoka, and T. Uesugi, Appl. Phys. Exp. **10**, 016501 (2017).
[10] H. Sakurai, M. Omori, S. Yamada, Y. Furukawa, H. Suzuki, T. Narita, K. Kataoka, M. Horita, M. Bockowski, J. Suda, and T. Kachi, Appl. Phys. Lett. **115**, 142104 (2019).

[11] T. Narita, H. Sakurai, M. Bockowski, K. Kataoka, J. Suda, and T. Kachi, Appl. Phys. Express **12**, 111005 (2019).
[12] A. G. Jacobs, B. N. Feigelson, J. K. Hite, C. A. Gorsak, L. E. Luna, T. J. Anderson, and F. J. Kub, Phys. Stat. Sol. A **217**, 1900789 (2020).
[13] R. Krause-Rehberg and H. S. Leipner, Positron Annihilation in Semiconductors, Solid-State Sciences (Springer-Verlag, Berlin, 1999) vol. 127.
[14] F. Tuomisto and I. Makkonen, Rev. Mod. Phys. **85**, 1583-1631 (2013).
[15] K. Saarinen, T. Laine, S. Kuisma, J. Nissilä, P. Hautojärvi, L. Dobrzynski, J. M. Baranowski, K. Pakula, R. Stepniewski, M. Wojdak, A. Wysmolek, T. Suski, M. Leszczynski, I. Grzegory, and S. Porowski, Phys. Rev. Lett. **79**, 3030-3033 (1997).
[16] K. Saarinen, T. Suski, I. Grzegory, and D. C. Look, Phys. Rev. B **64**, 233201 (2001).
[17] A. Uedono, S. F. Chichibu, Z. Q. Chen, M. Sumiya, R. Suzuki, T. Ohdaira, T. Mikado, T. Mukai, and S. Nakamura, J. Appl. Phys. 90, 181-186 (2001).
[18] J. Oila, J. Kivioja, V. Ranki, K. Saarinen, D. C. Look, R. J. Molnar, S. S. Park, S. K. Lee, and J. Y. Han, Appl. Phys. Lett **82**, 3433-3435 (2003).
[19] A. Uedono, H. Sakurai, T. Narita, K. Sierakowski, M. Bockowski, J. Suda, S. Ishibashi, S. F. Chichibu, and T. Kachi, Sci. Reports **10**, 17349 (2020).
[20] A. Uedono, H. Sakurai, J. Uzuhashi, T. Narita, K. Sierakowski, S. Ishibashi, S.F. Chichibu, M. Bockowski, J. Suda, T. Ohkubo, N. Ikarashi, K. Hono, and T. Kachi, Phys. Stat. Sol. B **259**, 2200183 (2022).
[21] K. Sierakowski, R. Jakiela, B. Lucznik, P. Kwiatkowski, M. Iwinska, M. Turek, H. Sakurai, T. Kachi, and M. Bockowski, Electronics **9**, 1380 (2020).
[22] A. van Veen, H. Schut, M. Clement, J. M. M. de Nijs, A. Kruseman, and M. R. IJpma, Appl. Surf. Sci. **85**, 216-224 (1995).
[23] S. Ishibashi, T. Tamura, S. Tanaka, M. Kohyama and K. Terakura, Phys. Rev. B **76**, 153310 (2007).
[24] S. Ishibashi, A. Uedono, H. Kino, T. Miyake, and K. Terakura, J Phys. Condens. Matter **31**, 475401 (2019).
[25] A. Uedono, S. Takashima, M. Edo, K. Ueno, H. Matsuyama, H. Kudo, H. Naramoto, and S. Ishibashi, Phys. Stat. Sol. B **252**, 2794–2801 (2015).
[26] A. Uedono, S. Takashima, M. Edo, K. Ueno, H. Matsuyama, W. Egger, T. Koschine, C. Hugenschmidt, M. Dickmann, K. Kojima, S. F. Chichibu, and S. Ishibashi, Phys. Stat. Sol. B **255**, 1700521 (2018).
[27] A. Uedono, H. Iguchi, T. Narita, K. Kataoka, W. Egger, T. Koschine, C. Hugenschmidt, M. Dickmann, K. Shima, K. Kojima, S. F. Chichibu, and S. Ishibashi, Phys. Stat. Sol. B **256**, 1900104 (2019).
[28] J. F. Ziegler, M. D. Ziegler, and J. P. Biersack, Nucl. Inst. Meth. B **268**, 1818 (2010).
[29] A. Castiglia, J. F. Carlin, and N. Grandjean, Appl. Phys. Lett. **98**, 213505 (2011).
[30] J. L. Lyons, A. Janotti, and C. G. Van de Walle, Phys. Rev. Lett. **108**, 156403 (2012).
[31] D. Lee, B. Mitchell, Y. Fujiwara, and V. Dierolf, Phys. Rev. Lett. **112**, 205501 (2014).
[32] A. Uedono, R. Tanaka, S. Takashima, K. Ueno, M. Edo, K. Shima, K. Kojima, S. F. Chichibu, and S. Ishibashi, Sci. Rep. **11**, 20660 (2021).
[33] E. Kano, K. Kataoka, J. Uzuhashi, K. Chokawa, H. Sakurai, A. Uedono, T. Narita, K. Sierakowski, M. Bockowski, R. Otsuki, K. Kobayashi, Y. Itoh, M. Nagao, T. Ohkubo, K. Hono, J. Suda, T. Kachi, and N. Ikarashi, J. Appl. Phys. **132**, 065703 (2022).